

Microstructures and Magnetism of Silicon co-implanted with Manganese and Carbon ions

This article has been downloaded from IOPscience. Please scroll down to see the full text article.

2011 J. Phys.: Conf. Ser. 281 012030

(<http://iopscience.iop.org/1742-6596/281/1/012030>)

View [the table of contents for this issue](#), or go to the [journal homepage](#) for more

Download details:

IP Address: 184.91.191.62

The article was downloaded on 15/04/2011 at 13:50

Please note that [terms and conditions apply](#).

Microstructures and Magnetism of Silicon co-implanted with Manganese and Carbon ions

L Chow¹, R R Vanfleet², M B Huang³, J LaRose³, E Del Barco¹, M Arcuri¹ and H Khallaf¹

¹Department of Physics, University of Central Florida, Orlando, FL 32816-2385, USA

²Department of Physics and Astronomy, Brigham Young University, Provo, UT 84602, USA

³College of Nanoscale Science and Engineering, University at Albany-SUNY, Albany, NY 12203, USA

E-mail: chow@mail.ucf.edu

Abstract. Dilute magnetic semiconductors based on transition metal doped silicon have attracted intense interest in recent years due to their compatibility with current silicon technology. Here we present transmission electron microscopy, secondary ion mass spectrometry and ferromagnetic resonance studies of silicon implanted with 1×10^{16} ions/cm² of Mn ions and silicon co-implanted with both 1×10^{16} ions/cm² of Mn ions and 2×10^{16} ions/cm² of carbon ions at a substrate temperature of 350 °C. Afterward, the samples were annealed at temperatures between 800 and 1000°C. The SIMS results show a marked difference between the two specimens while the TEM results show similar features in terms of Mn precipitation and particle evolution. The carbon implanted specimens show additional features that appear to be amorphous silicon pockets within the crystalline implant region. Only one specimen (Mn only implant, unannealed) showed any ferromagnetic properties.

1. Introduction

Magnetic semiconductors have been investigated since the early 1960s [1]. However, interests in magnetic semiconductors gradually waned in the 70s and 80s. In the late 1990s, when spintronic devices were proposed [2,3], magnetic semiconductors become an active research topic again. In particular, spintronic devices based on magnetic semiconducting oxides [4,5] and III-V compound semiconductors [6,7] have been shown with T_c above room temperature. Spintronic devices based on Mn-doped silicon are very desirable due to its compatibility with current silicon technology. In the last several years, both MBE grown Mn_xSi_{1-x} thin films [8] and Mn ion implanted silicon [9] have shown large magnetic moments associated with Mn ions. Since then, there have been many reports that tried to understand the basic mechanism which induced the large magnetic moment in Mn doped silicon [10–16].

Here we compared the microstructures and magnetic behaviour of silicon hosts implanted with only Mn ions and silicon samples co-implanted with Mn and C ions. It was reported recently that ferromagnetism can be obtained by implantation of carbon ions in antiferromagnetic Mn_5Si_3 [17]. It is known that the addition of ligands can change the lattice occupation of an impurity atom. For example, co-doped carbon ions can shift the lattice location of ion implanted erbium from the tetrahedral interstitial site to the hexagonal interstitial site in silicon [18, 19]. Here we investigated the

effect of carbon co-implantation on the depth profiles and clustering of Mn ions after high temperature annealing.

2. Experimental

In this work, we investigate effects of co-doped carbon impurities on the structural and magnetic properties of Si:Mn, in a hope to identify and tailor the possible microstructures responsible for ferromagnetism in Si. The silicon samples used in this experiment were cut from a float zone (FZ) Si (100) wafer (B-doped with resistivity 1-10 Ohm cm). Carbon atoms at 0.25 at. % are uniformly doped within the 250-nm surface layer of Si (100) using ion implantation and thermal annealing. The carbon ion implantations were conducted at room temperature, with energies of 30, 55 and 87 keV, and doses of 5×10^{15} , 5×10^{15} and 1×10^{16} cm⁻², respectively. The carbon ion ranges at these energies are estimated to be 97, 167 and 248 nm, respectively. The C-rich Si and Si control are subsequently implanted at 350°C with two Mn implants, one with an energy of 120 keV and a dose of 3.7×10^{15} cm⁻², and the other with an energy of 215 keV and dose of 6.3×10^{15} cm⁻². The Mn ion ranges are estimated to be 108 and 188 nm, respectively. The ion range estimates are based on room temperature SRIM calculations and may be shorter than achieved when the substrate is heated during implantation. Implantations were done at an angle of 5-7° from normal to minimize ion channelling. In addition, Mn implantations were conducted following C ion implantations. However, due to radiation induced diffusion [20, 21], particularly with the samples maintained at an elevated temperature of 350°C during Mn implantations, it is possible for Mn ions to stop at greater depths. Following Mn ion implantation, thermal annealing is conducted in the range of 800-1000°C for 30 minutes.

The secondary ions mass spectrometry (SIMS) was carried out at the Material Characterization Facility at the University of Central Florida with a CAMECA IMS-3f magnetic sector analyzer. Details of the SIMS measurements can be found in [22]. Transmission electron microscopy specimens were prepared in a cross sectional geometry by tripod polishing. A Tecnai TF20 in both TEM and STEM modes was used to study the samples. Some of the work was done using instruments at Brigham Young University and some on the microscope at the University of Western Cape, Cape Town, South Africa. Energy Dispersive X-ray spectroscopy (EDX) and electron energy loss spectroscopy (EELS) was used to identify the chemical composition of the precipitates.

Ferromagnetic resonance measurements were conducted at room temperature by employing a broad-band ($f = 1 \sim 40$ GHz) coplanar waveguide (CPW) [23] in the transmission mode as an inductive sensor and a 1.4 T electromagnet able to rotate in a plane. The CPW is made of 300 nm thick gold deposited on an undoped GaAs substrate. The sample is placed upside-down on top of the central sensing area of the CPW to achieve the best coupling.

3. Results and discussion

3.1. Secondary ions mass spectrometry

Figure 1 shows the Mn ion distribution of samples A and B as-implanted and after anneals between 800 and 1000°C, as measured by SIMS. The general features of the manganese ion distributions seem to be quite similar to our previous works [9, 13], namely the Mn as-implanted sample (Sample B) in figure 1(b) shows a featureless broad distribution with a long tail, resulting from multiple implantation and hot implantation. After annealing at temperatures between 800 and 1000°C, the profiles of Mn ions become much narrower and multiple peaks appear. We found that the Mn distributions of the annealed co-implanted samples (Samples A) seem to be narrower than the annealed Mn implanted samples (Samples B) as shown in figure 1. The double-peak profiles of both annealed samples (A and B) may be due to the double Mn implantation.

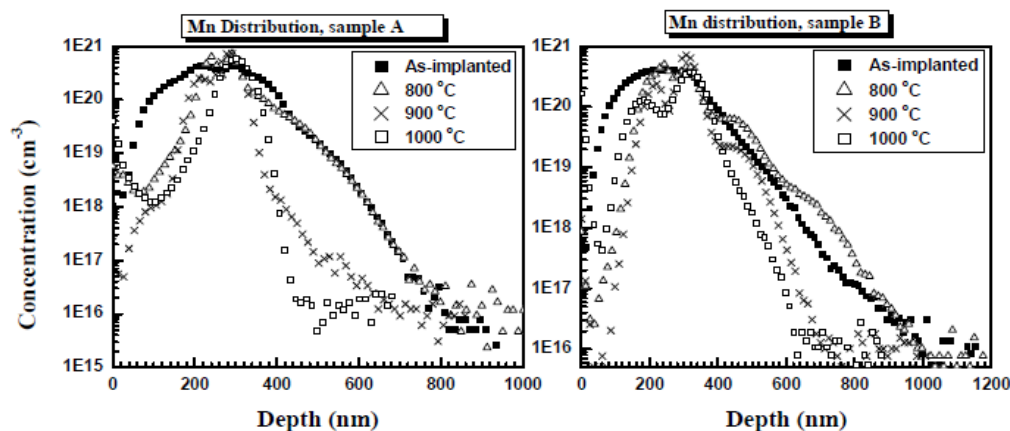


Figure 1. SIMS depth profiles of Mn ions in (a) Mn and Carbon co-implanted silicon, (Sample A), and (b) Mn implanted silicon (Sample B).

3.2. Transmission electron microscopy

The TEM results showed that all samples we investigated were crystalline. No amorphous layer was produced because the implantation was carried out at an elevated temperature (350 °C). Figure 2 shows the as-implanted sample, B-1, has many small precipitates which are confirmed by EDX to be the only regions where Mn is found. This precipitation is in contrast to low temperature implantations where no precipitates are found in the as-implanted specimens. This precipitation indicates that Mn ions are rather mobile at the implantation temperature of 350°C. The precipitate distribution is from a depth of 150 nm to about 400 nm below the surface of the silicon wafer. In a closer view (figure 2(b)), we see that these precipitates have a wide size distribution, ranging from smaller clusters (~ 4 nm) near the surface to larger clusters (up to 14 nm) near the End of Range (EOR) defects. The state, metallic or silicide, of these precipitates is not determined.

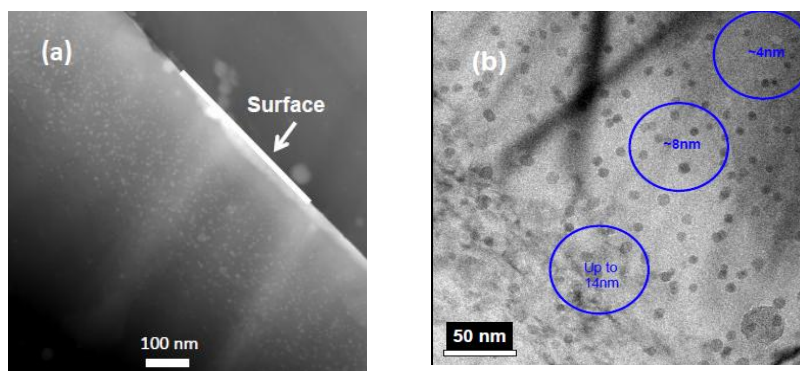


Figure 2. (a) As-implanted Si:Mn sample B-1. The ion implantation was carried at 350°C. Small Mn clusters were formed at depths between 150 to 400 nm. (b) A close-up image showed a distribution of the diameters of these Mn clusters from 4 to 14 nm.

For the sample annealed at 800°C (B-2, figure 3(a)), we noted that the precipitates seem to grow larger and start to transform from a circular shape into a faceted crystallite shape. In a close-up image (Figure 3(b)), fringes are clearly seen. These are Moire fringes that arise from the interference between periodicities in the silicon of the substrate and those in the precipitates.

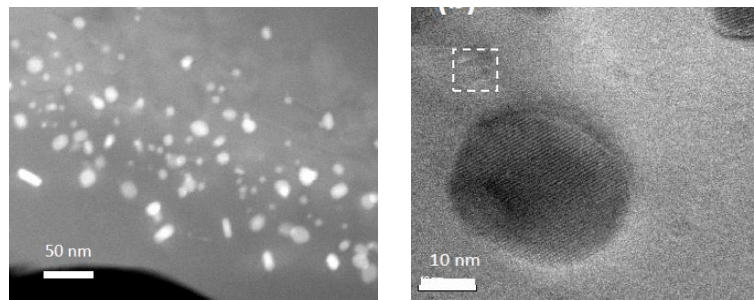


Figure 3. (a) ADF STEM image and (b) Bright Field TEM image of the Mn implanted sample B-2, annealed at 800°C.

For the co-implanted samples, we will detail our findings below for the as-implanted sample (A-1) and for the 800°C annealed sample (A-2). As shown in figure 4(a), the co-implanted sample showed no amorphous regions. Near the EOR there are many crystal defects and in the implant region many precipitates and voids (or amorphous regions). In figure 4(b), an enlarged Annular Dark Field Scanning Transmission Electron Microscopy (ADF STEM) image is shown. In this mode the image is formed by scanning (in a rectangular pattern) a focused probe of electrons across the sample. This allows the ADF imaging mode that generally shows atomic number dependant contrast but can also (if detector angles are somewhat smaller) show some diffraction contrast. In this image we can see that there are two types of defects: those that show brighter intensity or higher average atomic number and are confirmed by EDX to contain Mn and those that appear darker indicating lower average atomic number or lack of crystallinity. No Mn is found in the darker features. Attempts to detect carbon in the dark precipitates by EELS proved negative. Similar spots are also seen after annealing in the A-2 sample (figure 5).

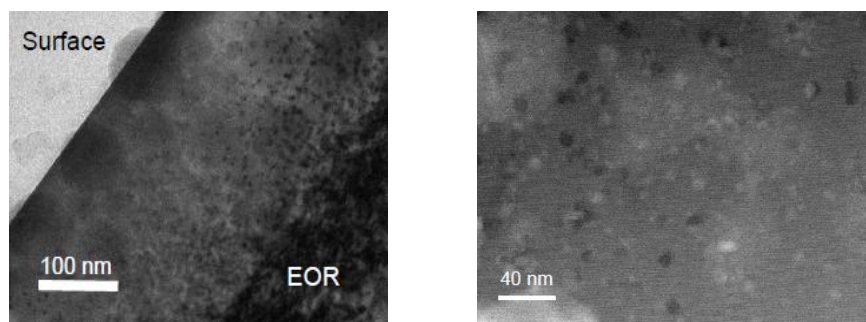


Figure 4. Silicon co-implanted with Mn and C ions (sample A-1). (a) TEM showing implant region with an EOR region full of lattice defects. (b) A higher magnification ADF STEM image showing bright (Mn precipitates) and dark features.

For the co-implanted and 800°C annealed sample (A-2), we noticed certain peculiar features as shown in figure 5(a). We see the typical EOR defects and Mn precipitates (in the 10's of nm ranges) similar to the B-2 sample. We also observed a few very dark spots and many small spots (examples are circled in figure 5(a)). Figure 5(b) is an ADF STEM image. In this view, the very dark spots in the TEM image of figure 5(a) are bright, the Mn precipitates are of medium brightness while many of the small spots show both bright and dark regions. Using EDX, we identify the very dark spots in figure 5(a) and the bright portions of the small spots as Ag precipitates. Silver paint was used to mount the silicon substrate during hot implantation to ensure good thermal contact. We do not expect

Ag to contaminate the silicon substrate during hot implantation and after implantation the silicon substrate was acid washed to remove all silver residues before the high temperature annealing. It appeared that this particular sample (A-2) still had some silver residue when the high temperature anneal was carried out. The many small spots in figures 5(a) and (b) have two types, those that have an associated Ag precipitate and many that do not (usually near the EOR or below). Both types of spots are dark in the STEM image and the dark regions contain no measurable concentration of any element other than silicon. As there is no significant drop in the silicon content (as measured by EELS) at these features, we identify them in both the annealed and as-implanted samples as amorphous silicon pockets associate with carbon co-implantation. The association with carbon implantation would imply some sort of carbon or carbon-silicon precipitation. This would match well with the observed ADF image contrast. However, no excess carbon content was observed by EELS in these dark regions. This would imply a low concentration of carbon that is undetectable in comparison to the background levels of carbon on the specimen or an actual lack of carbon. The exact nature of the formation of this feature is not understood at this time.

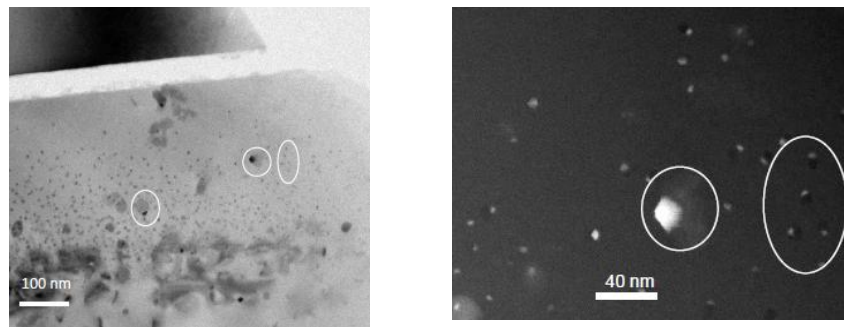


Figure 5. Mn and C co-implanted sample A-2. (a) TEM image shows some very dark spots (two marked with circles). (b) An ADF STEM image. The circled bright spots in (b) correspond to the right most circled dark spots in (a).

3.3. Ferromagnetic resonance spectroscopy

Ferromagnetic resonance measurements were carried out for the eight samples we prepared (A-1 through A-4, and B-1 through B-4). Seven samples showed null results. The only sample that showed a clear FMR signal is the B-1 sample. As shown in figure 6(a), a clear FMR signal is observed in the absorption spectrum at 2.3 kG when a 18 GHz microwave is used. At this frequency, the electron paramagnetic resonance (EPR) peak expected from isolated Mn-ions would be around 6 kG. Therefore the absorption we observed should be ascribed to the dynamics of a rigid magnetic vector resulting from exchange coupling. When the magnetic field is applied in the plane of the substrate, the frequency dependence of the resonance field is expected to follow a straight line when plotted as f^2/H vs H (as observed in figure 6), according to the in-plane FMR resonance condition,

$$\left(\frac{f}{2\pi\gamma} \right)^2 = H_R (H_R + 4\pi M_{\text{eff}}) \quad (1)$$

where the zero field intercept gives $4\pi M_{\text{eff}}$. The slope, which is the gyromagnetic ratio γ , can be used to obtain information of the Lande g -factor.

From our results, we obtained $g = 2.225$ and $M_{\text{eff}} = 1.350 \text{ emu/cm}^3$. We also carried out FMR measurements as a function of angle with respect to the normal of the substrate. The result is shown in figure 6(b). This result indicates a strong planar magnetostatic energy, likely related to an extended ferromagnetic film embedded inside the silicon substrate.

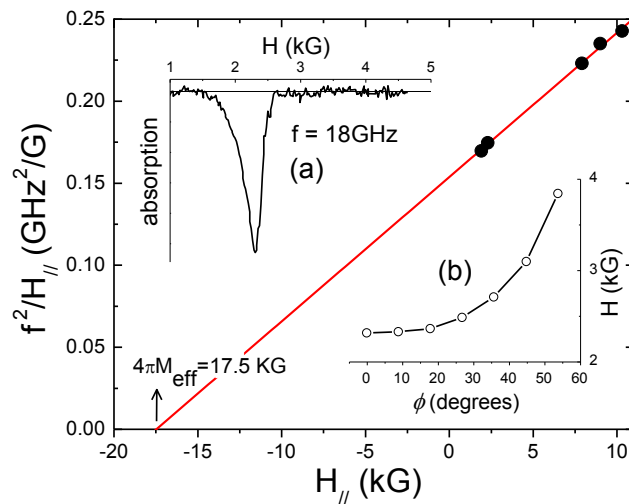


Figure 6. Frequency dependence of the FMR resonance peak with the magnetic field applied in the plan of the substrates. Inserts: (a) FMR spectrum obtained at 18 GHz. (b) Angular dependence of the FMR peak for the same frequency.

4. Conclusion

In summary, we have performed Mn and C ion co-implantation into silicon substrate to compare their physical properties with Mn ion implanted silicon samples. After annealing at different temperatures, we carried out SIMS, TEM and FMR measurements to compare Mn profiles, defect structures and magnetism of these samples. Our SIMS measurements show that the Mn profiles after high temperature annealing seem to be narrower for the co-implanted samples. The TEM measurements show typical EOR defects and Mn precipitates in both Mn implanted and C and Mn co-implanted samples. The co-implanted specimen showed small dark (in ADF STEM) features that appear to be amorphous silicon pockets. These have only been seen in the C implanted specimens. One co-implanted and annealed sample (A-2) showed Ag contamination. After an 800°C anneal, the Ag ions and Mn ions seem to form bi-precipitates. The FMR measurements showed only one sample (B-1) is ferromagnetic at room temperature. It appears that more experiments are needed to resolve the mystery of the magnetism in Si:Mn systems.

References

- [1] Tsubokowa I 1960 *J. Phys. Soc. Japan* **15** 1664
- [2] Ohno Y, Young DK, Beschoten B, Matsukura F, Ohno H and Awschalom DD 1999 *Nature* **402** 790
- [3] Wolf SA, Awschalom DD, Buhrman RA, Daughton JM, von Molnar S, Roukes ML, Chtchelkanova AY and Treger DM 2001 *Science* **294** 1488
- [4] Pearton SJ, Heo WH, Ivill M, Norton DP and Steiner T 2004 *Semicon. Sci. Technol.* **19** R59
- [5] Chambers SA, Droubay TC, Wang CM, Rosso KM, Heald SM, Schwartz DA, Kittilstved KR and Gamelin DR 2007 *Materials Today* **9** 28
- [6] Ohno H, Shen A, Matsukura F, Oiwa A, Endo A, Katsumoto S and Iye Y 1996 *Appl. Phys. Lett.* **69** 363
- [7] Beschoten B, Crowell PA, Malajovich I, Awschalom DD, Matsukura F, Shen A and Ohno H 1999 *Phys. Rev. Lett.* **83** 3073
- [8] Zhang F M, Liu X C, Gao J, Wu XS, Du YW, Zhu H and Xiao JQ 2004 *Appl. Phys Lett.* **85** 786
- [9] Bolduc M, Awo-Affouda C, Stollenwerk A, Huang MB, Ramos FG, Agnello G and LaBella VP 2005 *Phys. Rev. B* **71** 033302

- [10] Zhou SQ, Potzger K, Zhang GF, Mucklish A, Eichhorn F, Schell N, Grotzschel R, Schmidt B, Skorupa W, Helm M, Fassbender J and Geiger D 2007 *Phys. Rev. B* **75**, 085203
- [11] Lin HT, Huang WJ, Wang SH, Lin HH and Chin HS 2008 *J. Phys.: Condens. Mater.* **20** 095004
- [12] Zeng L, Helgren E, Rahimi M, Hellman F, Islam R, Wilkens B J, Culbertson RJ and Smith DJ 2008 *Phys. Rev. B* **77** 073306
- [13] Chow L, Gonzalez JC, Del barco E, Vanfleet R, Misiuk A, Prujarczyk M, Shunmugavelu A, Chai G and Bak-Misiuk J 2009 *J. Mater. Sci: Mater Electron* **19** S253
- [14] Misiuk A, Bak-Misiuk J, Surma B, Osinniy W, Szot M., Story T and Jagielski J 2006 *J. Alloys Comp.* **423** 201
- [15] Misiuk A, Barcz A, Bak-Misiuk J, Romanowski P, Chow L and Choi E 2009 *Mater. Sci. Eng. B* **159-160** 361
- [16] Shaughnessy M, Fong CY, Snow R, Liu K, Pask JE and Yang LH 2005 *Appl. Phys. Lett.* **95** 022515
- [17] Surgers C, Potzger K, Strache T, Moller W, Fischer G, Joshi N and v. Lohneysen H 2008 *Appl. Phys. Lett.* **93**, 062503
- [18] Ren XT and Huang MB 2006 *J. Appl. Phys.* **100** 023525
- [19] Huang MB and Ren XT 2002 *Appl. Phys. Lett.* **81** 2734.
- [20] Pearton SJ, Williams JS, Short KT, Johnson ST, Jacobsen DC, Poate JM, Gibson JM and Boerma DO 1989 *J. Appl. Phys.* **65** 1089
- [21] Dzhafarov TD 1989 *Phys. Stat. Sol. (b)* **155** 11
- [22] Francois-Saint-Cyr H, Anoshkina E, Stevie F, Chow L, Richardson K and Zhou D 2001 *J. Vac. Sci. Technol. B* **19** 1769
- [23] Quddusi HM, Ramsey CM, Gonzalez-Pons JC, Henderson JJ, del Barco E, de Loubens G and Kent AD 2008 *R. Sci. Instrum.* **79** 074703